IEEE Access
Multidisciplinary | Rapid Review | Open Access Journal

SPECIAL SECTION ON ADVANCED MODELING AND CONTROL OF COMPLEX MECHATRONIC SYSTEMS WITH NONLINEARITY AND UNCERTAINTY

Received August 29, 2017, accepted September 26, 2017, date of publication October 5, 2017, date of current version October 25, 2017.

Digital Object Identifier 10.1109/ACCESS.2017.2759579

Adaptive Fractional Order Terminal Sliding Mode Control of a Doubly Fed Induction Generator-Based Wind Energy System

NASIM ULLAH[1], MUHAMMAD ASGHAR ALI[2], ASIER IBEAS[3,4], AND JORGE HERRERA[4,5]

[1]Department of Electrical Engineering, CECOS University of Emerging Science and Information Technology, Peshawar 25124, Pakistan
[2]Department of Electrical Engineering, Qurtuba University of Science and Information Technology, Dera Ismail Khan 29050, Pakistan
[3]Escola d'Enginyeria, Autonomous University of Barcelona, 08193 Barcelona, Spain
[4]Departamento de Ingeniería, Universidad de Bogotá Jorge Tadeo Lozano, Bogotá 110311, Colombia
[5]Departamento de Electrónica y Telecomunicaciones, Facultad de Ingenierías, Instituto Tecnológico Metropolitano, Medellín 050034, Colombia

Corresponding author: Nasim Ullah (nasimullah@cecos.edu.pk)

This work was supported by University Jorge Tadeo Lozano under Grant 644-11-14. The work of A. Ibeas was supported in part by the Spanish Ministry of Economy and Competitiveness under Grant DPI2016-77271-R and in part by University of the Basque Country (UPV/EHU) under Grant PPG17/33.

ABSTRACT The dynamic model of a doubly fed induction generator (DFIG)-based wind energy system is subjected to nonlinear dynamics, uncertainties, and external disturbances. In the presence of such nonlinear effects, a high-performance control system is required to guarantee the smooth and maximum power transfer from the wind energy system to the ac grids. This paper proposes a novel fractional order adaptive terminal sliding mode control system for both the rotor and grid side converters of the DFIG system. The stability of the closed loop is ensured using the fractional order Lyapunov theorem. Numerical results are presented to show the superiority of the proposed control method over the classical sliding mode control system and the proportional integral controllers.

INDEX TERMS Wind turbine doubly fed induction generator, active and reactive power control, fractional calculus, terminal sliding mode control.

I. INTRODUCTION

The availability of energy resources play vital role in the economic growth of a region. During the last few decades', annual power demands around the globe have been increased considerably due to the industrial revolution and improved standard of livings. However due to this rapid development, modern world is facing the problems of greenhouse gases and toxic wastes. Clean and pollution free renewable form of the energy production has now become the key objective for all the power producing industries. Wind is a reliable, cheap and clean energy source. Wind energy systems are consistent, cost effective and pollution free. Doubly Fed Induction Generator (DFIG) plays a vital role in the modern variable speed wind energy conversion systems and it is a widely utilized power generating component in the modern wind farms. Use of the DFIG offers many advantages, such as variable speed operation, torque control, low inverter cost and the flexibility of four quadrant active and reactive power control capabilities [1]. Adding to this fact, the total installed capacity of the wind power around the world has reached to 318 GW in 2013 [2], [3]. Wind turbine manufacturers are striving to develop larger wind turbines in the range of 3–6 MW. These large wind turbines are all based on the variable speed operation. Variable speed operation in comparison with constant speed offer less stresses over the mechanical structures, offers direct control over active and reactive powers and reduction in acoustic noise [4].

Development of the control system for DFIG based variable speed wind turbines is an important task and a lot of research work has been carried out regarding the improvements of the control loop performance. The system's performance under the proportional integral (PI) control mostly depends on the system's parameters as well as accurate tuning of the control gains. Vector control using Proportional Integral (PI) controller is mostly used for the control of the DFIG based wind energy systems [5]–[7]. However the systems with linear control methods show poor performance due to the presence of inherent nonlinearities and un-modeled dynamics. Apart from the linear controllers there are many other methods that have been suggested in the literature.

Predictive power control of DFIG is proposed in [8]. In [9] a robust state feedback control method is proposed to effectively compensate the disturbances in the input dynamics. In [9] the simulation results with the state feedback control clearly demonstrated the effective cancellation of the disturbances in the system input matrices. Comparative study of the classical PID and the robust H_∞ control is presented in [10]. As compared to the classical PI control, the trajectories of the state feedback control system converge much faster. Several researchers proposed artificial intelligence (AI) methods such as fuzzy system and neural networks for the rotor and grid side converters of the DFIG system. Fuzzy systems and artificial neural networks have the ability to approximate the nonlinearities of a system with model free approach. As a result, it can be a good choice for the control of nonlinear systems such as DFIG based wind energy systems. In [11] an artificial neural network based robust tracking control is derived and the results are compared with classical PI controller. From the presented results, it is concluded that the neural network based control system is more robust against the parametric uncertainty. In [12] for DFIG based wind power system, the authors have proposed two variants of the controllers based on the fuzzy logic system. It was concluded from the simulation results that the fuzzy logic controllers ensure superior performance as compared to the PID in the presence of the system's uncertainties. There are several challenges in the implementation of the intelligent control systems. The challenges include the appropriate rules selection, choosing number of neurons and the selection of hidden layers. In [13] an adaptive robust control approach is investigated for the rotor and grid side converters of the DFIG based wind energy system. The proposed control scheme guarantees generator velocity tracking error to remain in the bounds even in the presence of uncertainties. In the DFIG systems, uncertainties and external disturbances may cause variations in the closed loop response. In this regard, the variable structure control such as classical sliding mode control (SMC) has been identified as the most suitable alternative approach [14].

In [15] and [16], classical first order sliding mode controllers has been proposed for the active and reactive power loops of the DFIG based wind turbine systems. In [17] the recursive back stepping terminal sliding mode controller is proposed for a DFIG based system with maximum wind energy capture. For the classical first order SMC, it is very vital to choose an accurate hyper plane that will ensure convergence and asymptotic stability for the nonlinear system like DFIG. The inherent chattering phenomenon associated with classical sliding mode controller is highly undesirable. There are several techniques to suppress the chattering problem in the classical SMC. In [18] a nonlinear sliding surface based fast and adaptive terminal sliding mode control strategy is proposed for the active power control of a DFIG based system. Moreover, to minimize the chattering effect several hybrid control techniques have been proposed such as fuzzy SMC, adaptive SMC and higher order SMC [19]–[23]. In [19] and [19] fuzzy SMC based controllers are used for the rotor side converter of the DFIG based system. The output response of the system accurately tracks the reference signal and is sensitive to the undesired perturbations. In [20] and [21] a robust higher order sliding mode control is proposed. The discontinuous term in the higher order sliding mode control approach is integrated, thus the chattering effect is minimized in the process without altering the system robustness. In [22] a maximum power point tracking based higher order sliding mode control is proposed for the DFIG based wind energy system. In [23] and [37]–[39] novel adaptive higher order sliding mode control system is proposed for the DFIG based wind energy conversion system. Chattering is efficiently minimized by utilizing the higher order SMC control techniques, however tuning the parameters of the higher order sliding mode controllers is a challenging task, as the parameter values depend primarily on the known initial conditions.

The control methods discussed so far are integer order. Recently fractional order control has emerged as a promising research area and is being widely applied to both linear and nonlinear systems [2], [24]. In [2] and [24]–[29], the non integer controllers are proposed for the nonlinear systems. The basic theory of fractional order differentiation and fractional order integration is well explained in [25] and [26]. In comparison to the integer order SMC, the fractional order sliding mode controller offers more degree of freedom due to its additional design parameters [27]. Hence, the fractional orders can be tuned for the optimum dynamic response, while the robustness remains unchanged. The stability of the fractional order systems is derived and discussed in [28]. Moreover, in [29] fractional order Lyapunov theorem is proposed for deriving the fractional order controllers and ensuring the stability. Apart from the normal operation, several researchers have focused their work on the fault tolerance aspect of the controller and system loops. This topic needs further exploration as all grid connected wind farms have to fulfill the grid code strictly [40]. Hence the proposed controllers should be robust as well as capable of ensuring the normal performance of the system under faults [41], [42].

Based on the above discussed literature, this article formulates a novel fractional order terminal sliding mode controller for the active and reactive power loops of the wind turbine based doubly fed induction generator system. The Mathematical model is subjected to nonlinearities, external disturbances and parameter variations. A nonlinear fractional order terminal sliding mode control is derived for the system mentioned above. Stability proof is derived using Fractional Lyapunov theorem. Finally, the performance of the proposed controller is compared with SMC and PI methods. The rest of the article is arranged as following. Section 2 is used to define the basic mathematical foundation; section 3 discusses the mathematical models of the wind energy system, section 4 models the DFIG generator, section 5 shows all the derivations related to the control schemes and the results are discussed in the section 6.

II. BASIC DEFINITIONS FOR FRACTIONAL CALCULUS

Fundamental fractional operator is defined as ${}_aD_t^{\alpha}$ [29].

$$aD_t^{\alpha} \cong D^{\alpha} = \begin{cases} \dfrac{d^{\alpha}}{dt^{\alpha}}, & R(\alpha) > 0 \\ 1, & R(\alpha) = 0 \\ \displaystyle\int_a^t (d\tau)^{-\alpha}, & R(\alpha) < 0 \end{cases} \tag{1}$$

Here α represents the order of the fractional operator and R(α) represents the set of real numbers. There are three definitions used for the general fractional operator [29].

Definition 1: The αth order Riemann–Liouville fractional derivative and integration of a function $f(t)$ with respect to t is given by

$${}_aD_t^{\alpha} f(t) = \frac{d^{\alpha}}{dt^{\alpha}} f(t) = \frac{1 d^m}{\Gamma(m-\alpha) dt^m} \int_{\alpha}^{t} \frac{f(\tau)}{(t-\tau)^{\alpha-m+1}} d\tau \tag{2}$$

$$aD_t^{-\alpha} f(t) = I^{\alpha} f(t) = \frac{1}{\Gamma(\alpha)} \int_{\alpha}^{t} \frac{f(\tau)}{(t-\tau)^{1-\alpha}} d\tau \tag{3}$$

Here m is the first integer larger than "a", such as $m - 1 < \alpha < m$, $t - \alpha$ is the interval of integration and G is Euler's Gamma function.

Definition 2: The αth order Caputo fractional derivative expression of a continuous function is expressed as [29].

$${}_aD_t^{\alpha} \cong D^{\alpha} = \begin{cases} \dfrac{1}{\Gamma(n-\alpha)} \displaystyle\int_{\alpha}^{t} \frac{f^n(\tau)}{(t-\tau)^{\alpha-n+1}} d\tau \\ \qquad (\mathrm{n}-1 \le \alpha < \mathrm{n}) \\ \dfrac{d^m}{dt^n} f(t) \quad (\alpha = \mathrm{n}) \end{cases} \tag{4}$$

Definition 3: The GL definition of order α is expressed as [29].

$${}_a{}^{GL}D_t^{\alpha} f(t) = \lim_{h \to 0} \frac{1}{h^{\alpha}} \sum_{j=0}^{[(t-\alpha)/h]} (-1)^j \binom{\alpha}{j} f(t - jh) \tag{5}$$

$$\binom{\alpha}{j} = \frac{\Gamma(\alpha+1)}{\Gamma(j+1)\Gamma(\alpha-j+1)} \tag{6}$$

Here h represents the time step and Γ (.) represents gamma function. The stability of the non-integer systems has been discussed in the literature with details [28], [31]. Oustaloup recursive approximation algorithm is used to approximate the fractional orders by classical integer order transfer function. The details of the Oustaloup recursive approximation algorithm [32].

III. WIND ENERGY CONVERSION SYSTEM MODEL

In this section the detailed nonlinear models for wind turbine, rotor and grid side converters are discussed. The detailed block diagram of the DFIG based wind turbine system is shown in Fig.1a [3].

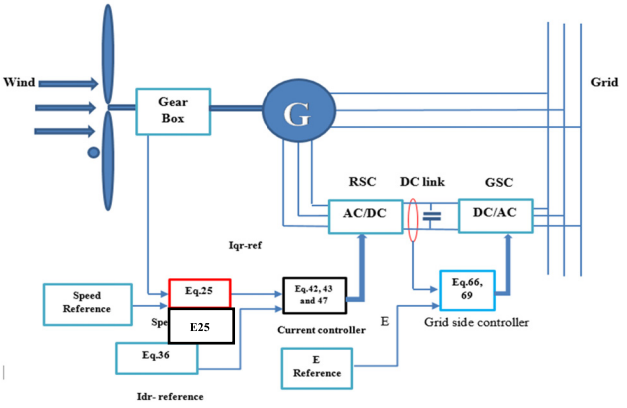

(a)

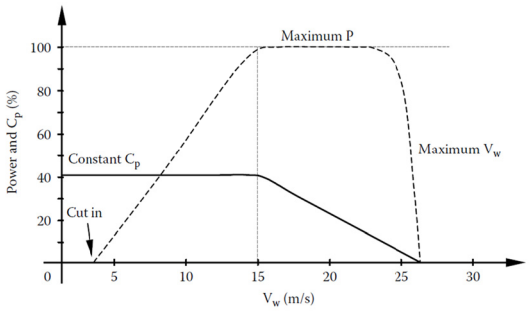

(b)

FIGURE 1. (a) Schematic of DFIG based wind turbine system (b) Wind turbine Ideal power curve.

MODELING OF WIND TURBINE

Wind turbine extracts kinetic energy from the wind and converts it to the mechanical energy for the DFIG. The power input from wind is [33],

$$P = \frac{1}{2}(air\ per\ unit\ time)(wind\ velocity)$$

The output mechanical power from the wind turbine to the DFIG system is given as $P = \frac{1}{2} C_p A v^3$. Total aerodynamic power extracted from the wind can be expressed as $P_t = \frac{1}{2} \rho A C_p v^3$. Where ρ is the air density in kg/m^3, A is the area of the turbine blades in m^2, C_p is the power coefficient that depends on shape and geometry of the turbine blades. C_p is a nonlinear function of the pitch angle β and tip speed ratio λ Where $\lambda = \frac{\Omega_t R}{v}$, Ω_t is the wind turbine mechanical angular shaft speed in $rad/$ sec and R is the radius of the wind turbine rotor in meters. A typical relationship between C_p, power and wind speed is shown in Figure 1b [33]. The expression between C_p and λ is expressed in Eq. (7).

$$C_p = c_1 \left(\frac{c_2}{\lambda} - 1 \right) e^{\frac{-c_3}{\lambda}} \tag{7}$$

In Equation (7), c_1, c_2 and c_3 are the constants. The power coefficient C_p converts only 59% of wind kinetic energy to the mechanical energy [34]. For a particular speed, when the output power of the wind turbine is maximum, then at this

speed the tip speed ratio corresponds to λ_{opt}. When $\lambda = \lambda_{opt}$ the power coefficient is maximum i.e. ($C_p = C_{p-\max}$), thus maximum power can be extracted from the wind turbine [44]. Fig. 1b depicts the ideal power curve of a typical wind turbine [9]. From the power curve it can be noticed that in the range of the cut in wind speed up to 15m/s, the power coefficient remains constant. The torque of the wind turbine is given by $T_r = \frac{T_t}{G}\Omega_t = \frac{\Omega_r}{G}$. Here T_r and T_t are the generator's torque and aerodynamic torque respectively, G is the gear ratio and Ω_r is generator speed. The reference rotor speed and the grid power are expressed as

$$\Omega_{r-ref} = \frac{\lambda_{opt} G}{R} v \tag{8}$$

The speed reference defined in Eq. 8 is only applicable when the turbine is working on the maximum power point. In other cases the speed reference is calculated from the look up table and the power curve data [1]. More explanations on the wind turbine control strategies based on different speed regions are given by the authors of [1].

$$P_{grid-ref} = \frac{1}{2}\eta\rho\pi^2 C_{p-\max} v^3 \tag{9}$$

Here η is wind turbine efficiency.

IV. MODELING OF GENERATOR

In three phase plan, the representation of the asynchronous machine is difficult because it is strongly coupled. Equations describing DFIG model in synchronous (d-q) frame are given below: [35]

$$\begin{cases} V_{ds} = R_s I_{ds} + \dfrac{d}{dt}\varphi_{ds} - \omega_s \varphi_{qs} \\ V_{qs} = R_s I_{qs} + \dfrac{d}{dt}\varphi_{qs} + \omega_s \varphi_{ds} \\ V_{dr} = R_r I_{ds} + \dfrac{d}{dt}\varphi_{dr} - (\omega_s - \omega_r)\varphi_{qr} \\ V_{qr} = R_r I_{qs} + \dfrac{d}{dt}\varphi_{qr} + (\omega_s - \omega_r)\varphi_{dr} \end{cases} \tag{10}$$

Here $\varphi_{ds} = L_s I_{ds} + M I_{dr}$; $\varphi_{qs} = L_s I_{qs} + M I_{qr}$; $\varphi_{dr} = L_r I_{dr} + M I_{ds}$; $\varphi_{qr} = L_r I_{qr} + M I_{qs}$, $\omega_r = P\Omega_r$, V_{ds}, represents the d-axis and q-axis stator voltage components V_{qs}, V_{dr}, V_{qr} are the rotor voltage components, I_{ds}, I_{qs} are the stator current components, P is the number of pole pairs, I_{dr}, I_{qr} are the rotor current components, R_s, R_r are the stator and rotor resistances, φ_{ds}, φ_{qs} are the stator flux components, φ_{dr}, φ_{qr} are the rotor flux components L_s, L_r are the stator and rotor inductances, M is the magnetizing inductance and ω_s, ω_r are the stator and rotor angular velocities. The mechanical dynamics of the rotating parts are modeled as

$$J\frac{d}{dt}\Omega_r = T_{em} - T_r - f_r \Omega_r \tag{11}$$

Here J denotes the moment of inertia of the rotating parts f_r is the co-efficient of friction and T_{em} is electromagnetic torque of the DFIG. Eq. 11 represents the dynamics of the DFIG machine only. A more realistic approach is to use the two mass mechanical models for the DFIG and the turbine. The two mass models is expressed as [1]

$$\begin{aligned} J_t\frac{d}{dt}\Omega_t &= T_t - T_{em} - f_t\Omega_t \\ J_m\frac{d}{dt}\Omega_m &= T_{em} - f_m\Omega_m + T_{em} \\ \frac{d}{dt}T_{em} &= k_{tm}(\Omega_t - \Omega_m) + f_{tm}(\dot{\Omega}_t - \dot{\Omega}_m) \end{aligned} \tag{12}$$

In Eq. 12, J_m J_t denote the moment of inertia of the DFIG and the turbine respectively, f_m f_t represent the co-efficient of the friction in the DFIG and turbine side, Ω_m Ω_t represent the DFIG and turbine angles and T_{em} is electromagnetic torque of DFIG.

The Electromagnetic torque is expressed as $T_{em} = P\frac{M}{L_s}\left(\varphi_{qs} I_{dr} - \varphi_{ds} I_{qr}\right)$. To simplify the task, the nonlinear model expressed above is approximated as DC machine [36]. By orienting d-axis in the direction of flux φ_s we have $\varphi_{ds} = \varphi_s$, $\varphi_{qs} = 0$, therefore by using Eq. 12 one obtains

$$T_{em} = P\frac{MV_s}{\omega_s L_s} I_{qr} \tag{13}$$

If we neglect the per phase stator resistance and make the stator flux constant, the direct and quadrature voltage vectors on the stator axis can be written as $V_{ds} = 0$, $V_{qs} = V_s = \omega_s \varphi_s$. With this assumption and using (13) in (10) and (11) the direct and quadrature voltages on rotor axis and stator active and reactive power can be expressed in accordance to the rotor currents as follows.

$$\begin{cases} V_{dr} = R_r I_{dr} + \sigma L_r \dfrac{d}{dt} I_{dr} - \sigma L_r s \omega_s I_{qr} \\ V_{qr} = R_r I_{qr} + \sigma L_r \dfrac{d}{dt} I_{qr} + \sigma s \omega_s I_{dr} + s\dfrac{MV_s}{L_s} \end{cases} \tag{14}$$

$$\begin{cases} P_s = -\dfrac{MV_s}{L_s} I_{qr}; \quad Qs = \dfrac{V_s^2}{\omega_s L_s} - \dfrac{MV_s}{L_s} I_{dr} \end{cases} \tag{15}$$

Here $\sigma = 1 - \frac{M}{L_r L_s}$, $s = \frac{\omega_s - \omega_r}{\omega_s}$, where'$s$'' is the DFIG slip. Vector control strategy is used to control the DFIG based wind energy system. It is worth mentioning that Eq. 14 represents the 3 phase equivalent rotor side converter's model in d-q reference model. Since the active and reactive powers of the stator side directly depends on the d and q component of the rotor currents therefore the three phase quantities of the rotor side are converted to the two parameter systems using the Clark and park transformations. For simplicity the controllers are implemented in d-q reference frame and then using the inverse Park and Clark transform the actual 3 phase control signals are formed to drive the system [1]. The nonlinear system model can be represented in state space form given as under

$$\left[\begin{array}{l} \dot{x} = F(x) + Hu = f(x) + \Delta f + hu + \Delta hu \\ \quad = f(x) + hu + d \end{array}\right] \tag{16}$$

Where $x = [I_{dr}\ I_{qr}]^T$, $[u_1\ u_2] = [V_{dr}\ V_{qr}]^T$, f and h represent the nominal values of the F and H, Δf and Δh are the associated uncertainties in the plant and input vector,

$d = \Delta f + \Delta hu = [\, d_1 \;\; d_2 \,]^T$ represent the unknown lumped uncertainty in the plant model [2]. The nominal parameters of the systems are given in table 1, Appendix A. The nominal matrices of the function f and h are expressed as,

$$\begin{bmatrix} f_1(x) = -\dfrac{R_r}{\sigma L_r} I_{dr} + s\omega_s I_{qr}; \\ f_2(x) = -\dfrac{R_r}{\sigma L_r} I_{qr} - s\omega_s I_{dr} - s\dfrac{MV_s}{\sigma L_r L_s} \end{bmatrix}, \tag{17}$$

$$\begin{bmatrix} h_1 \\ h_2 \end{bmatrix} = \begin{bmatrix} \dfrac{1}{\sigma L_r} & 0 \\ 0 & \dfrac{1}{\sigma L_r} \end{bmatrix} \tag{18}$$

V. ROTOR SIDE AND GRID SIDE CONVERTER'S CONTROL

Based on the mathematical models described in the previous section, and from fig.1a, the system models can be divided into two subgroups, i.e. electrical and the mechanical subsystems. The control scheme consists of an outer loop speed controller and an inner-loop current controller. Since the electrical subsystem (inner loop) is faster than the mechanical subsystem (outer loop), a cascaded structure is assumed for the design of the controller. The inner loop is employed to regulate the d -axis rotor current and the electromagnetic torque, while the outer loop is used for the speed trajectory tracking. By comparing the control system discussed in [2], our proposed method is based on the novel fractional order continuous terminal sliding mode control method. Using fractional order Lyapunov method, non-integer adaptive laws are formulated. As compared to the work presented in [2], the proposed controllers exhibit the fastest convergence property, less chattering and enhanced robustness.

A. SPEED CONTROLLER

In this article the single and the two mass models are discussed as shown in Eq. 11 and 12. However the speed controller is formulated based on Eq. 11. In future the same concepts can be extended to derive and test the speed loop for the two mass model of Eq. 12. To derive the speed control loop based on simple model, Eq. 11 is represented as

$$\frac{d}{dt}\Omega_r = \frac{T_{em}}{J} + d_3 : \quad d_3 = -\frac{T_r}{J} - \frac{f_r \Omega_r}{J} \tag{19}$$

Where T_{em} is the control input, J is the best available approximate (nominal value) of moment of inertia, d_3 is the lumped uncertainty which represents aerodynamic torque, force of friction and parametric uncertainty. Choose the speed tracking error as $e_s = \Omega_r - \Omega_{r-ref}$. By replacing $\dot{\Omega}_r$ from (19) in the first derivatives of speed error yields expression (20)

$$\dot{e}_s = \dot{\Omega}_r - \dot{\Omega}_{r-ref}; \quad \dot{e}_s = \frac{T_{em}}{J} + d_3 - \dot{\Omega}_{r-ref} \tag{20}$$

A fractional order sliding surface is proposed and given in (21)

$$\begin{aligned} S_s &= c_5 D^{-\alpha} e_s + c_6 D^{\alpha} |e_s|^{\gamma} \operatorname{sgn}(e_s) \\ \dot{S}_s &= c_5 D^{1-\alpha} e_s + c_6 \gamma D^{\alpha} \underbrace{D^1 |e_s|^{\gamma} \operatorname{sgn}(e_s)} \end{aligned}$$

$$\dot{S}_s = c_5 D^{1-\alpha} e_s + c_6 \gamma D^{\alpha} |e_s|^{\gamma-1} \dot{e}_s \tag{21}$$

Here c_5, c_6 and γ represent the constants. By applying $D^{-\alpha}$ to both sides of $\dot{S}_s$ in (21) yields

$$D^{1-\alpha} S_s = c_5 D^{1-2\alpha} e_s + c_6 \gamma |e_s|^{\gamma-1} \dot{e}_s \tag{22}$$

In the left hand side of Eq. 22, the operator $D^{1-\alpha}$ represents the fractional derivative term. For simplicity the operator $D^{1-\alpha}$ is represented as $D^{\bar{\alpha}}$. With this notation a more convenient form of the Eq.22 is written as

$$D^{\bar{\alpha}} S_s = c_5 D^{1-2\alpha} e_s + c_6 \gamma |e_s|^{\gamma-1} \dot{e}_s \tag{23}$$

By combining $\dot{e}_s$ from (20) in (23) one obtains

$$D^{\bar{\alpha}} S_s = c_5 D^{1-2\alpha} e_s + c_6 \gamma \begin{pmatrix} \dfrac{|e_s|^{\gamma-1} T_{em}}{J} + |e_s|^{\gamma-1} d_3 \\ -|e_s|^{\gamma-1} \dot{\Omega}_{r-ref} \end{pmatrix} \tag{24}$$

The control law can be defined as

$$\begin{cases} T_{em} = T_{em-eq} + T_{em-s} - \hat{\theta} \\ T_{em-eq} = J|e_s|^{1-\gamma} \{ |e_s|^{\gamma-1} \dot{\Omega}_{r-ref} - \dfrac{c_5}{\gamma c_6} D^{1-2\alpha}(e_s) \\ T_{em-s} = J|e_s|^{1-\gamma} (-\dfrac{k_{r3}}{\gamma c_6} (\operatorname{sgn}(S_s^p)) \end{cases} \tag{25}$$

Here k_{r3} represents the discontinuous switching gain which is usually chosen greater than the lumped uncertainty. From Eq. 24 the term $|e_s|^{\gamma-1} d_3 = \theta$ and $\hat{\theta}$ represents the estimated value as expressed in Eq. 25. The lumped uncertainty is estimated online and the adaptive law is derived from the stability proof as explained below.

Stability Proof 1: The Lyapunov candidate function is $V_s = \frac{1}{2} S_s^2 + \frac{1}{2\eta}(\theta - \hat{\theta})^2$. By applying the fractional operator $D^{\bar{\alpha}}$ to the function V_s yields

$$\begin{aligned} D^{\bar{\alpha}} V_s = {} & S_s D^{\bar{\alpha}} S_s + \frac{1}{\eta}(\theta - \hat{\theta}) D^{\bar{\alpha}} (\theta - \hat{\theta}) \\ & + \left| \sum_{j=1}^{\infty} \frac{\Gamma(1+\bar{\alpha})}{\Gamma(1-j+\bar{\alpha})\Gamma(1+j)} D^j S_s D^{\bar{\alpha}-j} S_s \right| \\ & + \left| \sum_{j=1}^{\infty} \frac{\Gamma(1+\bar{\alpha})}{\Gamma(1-j+\bar{\alpha})\Gamma(1+j)} D^j e_\theta D^{\bar{\alpha}-j} e_\theta \right| \end{aligned} \tag{26}$$

To complete the proof, the following in-equality is defined [29].

$$\left| \sum_{j=1}^{\infty} \frac{\Gamma(1+\alpha)}{\Gamma(1-j+\alpha)\Gamma(1+j)} D^j s D^{\alpha-j} s \right| \leq \lambda \, |s| \tag{27}$$

From Eq. 26, the error term is defined as $e_\theta = \theta - \hat{\theta}$. It is assumed that the unknown parameter θ in Eq. 25 is represented by its upper bound .i.e. constant so Eq. 26 can be simplified as

$$D^{\bar{\alpha}} V_s \leq S_s D^{\bar{\alpha}} S_s + \frac{1}{\eta}(\theta - \hat{\theta})(-D^{\bar{\alpha}} \hat{\theta}) + \lambda_1 |S_s| + \lambda_1 |e_\theta| \tag{28}$$

By combining Eq. 24, 25 and 28 one obtains

$$
\begin{aligned}
&D^{\bar{\alpha}}V_s \\
&\leq S_s[c_5 D^{1-2\alpha}e_s + c_6\gamma\begin{pmatrix}\frac{|e_s|^{\gamma-1}T_{em}}{J} + |e_s|^{\gamma-1}d_3 \\ -|e_s|^{\gamma-1}\dot{\Omega}_{r-ref}\end{pmatrix}] \\
&+\frac{1}{\eta}(\theta-\hat{\theta})(-D^{\bar{\alpha}}\hat{\theta}) + \lambda_1|S_s| + \lambda_1|e_\theta| \leq S_s[c_5 D^{1-2\alpha}e_s \\
&+c_6\gamma\begin{pmatrix}\frac{|e_s|^{\gamma-1}}{J}\{J|e_s|^{1-\gamma}\{|e_s|^{\gamma-1}\dot{\Omega}_{r-ref} - \frac{c_5}{\gamma c_6}D^{1-2\alpha}(e_s) \\ -\hat{\theta} - \frac{k_{r3}}{\gamma c_6}|e_s|^{1-\gamma}(\mathrm{sgn}(S_s^p)\} + \theta - |e_s|^{\gamma-1}\dot{\Omega}_{r-ref}\end{pmatrix}] \\
&+\frac{1}{\eta}(\theta-\hat{\theta})(-D^{\bar{\alpha}}\hat{\theta}) + \lambda_1|S_s| + \lambda_1|e_\theta| \qquad (29)
\end{aligned}
$$

Eq. (29) is further simplified as

$$
\begin{aligned}
D^{\bar{\alpha}}V_s \leq\ & -k_{r3}S_s|e_s|^{1-\gamma}(\mathrm{sgn}(S_s^p) + c_6\gamma S_s\left(\theta-\hat{\theta}\right) \\
&+\frac{1}{\eta}(\theta-\hat{\theta})(-D^{\bar{\alpha}}\hat{\theta}) + \lambda_1|S_s| + \lambda_1|e_\theta| \qquad (30)
\end{aligned}
$$

From Eq. 30, the following adaptive law is derived

$$
D^{\bar{\alpha}}\hat{\theta} = \eta c_6\gamma S_s \qquad (31)
$$

By combining Eq. 31 and 30 one obtains

$$
\begin{aligned}
D^{\bar{\alpha}}V_s \leq\ & -k_{r3}S_s|e_s|^{1-\gamma}(\mathrm{sgn}(S_s^p) + c_6\gamma S_s\left(\theta-\hat{\theta}\right) \\
&+\frac{1}{\eta}(\theta-\hat{\theta})(-D^{\bar{\alpha}}\hat{\theta}) + \lambda_1|S_s| + \lambda_1|e_\theta| \qquad (32)
\end{aligned}
$$

Eq. 32 can be represented in a more convenient form as

$$
D^{\bar{\alpha}}V_s \leq -k_{r3}S_s|e_s|^{1-\gamma}(\mathrm{sgn}(S_s^p) + \lambda_1|S_s| + \lambda_1|e_\theta| \qquad (33)
$$

By letting $k_{r3} \geq \lambda_1 + \lambda_2 + \psi$, the term $D^{\bar{\alpha}}V_s \leq 0$, As the lumped uncertainty is adapted online using the fractional order adaptive law of Eq. 31 so the discontinuous gain is : $k_{r3} \geq \lambda_1 + \lambda_2 + \psi$. Here ψ represents the small perturbation or the approximation error of the Eq. 31.

B. CURRENT CONTROLLER

The objective of this section is to derive a control expression such that the state x tracks the desired trajectory x_{ref} in the presence of uncertainties. The reference trajectory is defined as $x_{ref} = [\, I_{dr-ref} \;\; I_{qr-ref} \,]^T$. Based on (13) we have

$$
I_{qr-ref} = \frac{\omega_s L_s}{PMV_s}T_{em-ref} \qquad (34)
$$

The term T_{em-ref} of Eq. 34 is derived based on the speed controller of Eq. 25. The reactive power's reference is defined as

$$
Q_{s-ref} = \frac{V_s^2}{\omega_s L_s} - \frac{MV_s}{L_s}I_{dr}, \qquad (35)
$$

Set $Q_{s-ref} = 0$, then the reference d axis current is derived as

$$
I_{dr-ref} = \frac{V_s}{\omega_s M} \qquad (36)
$$

Current tracking errors are defined as

$$
\begin{aligned}
e = x - x_{ref} &= [\, e_1 \quad e_2 \,]^T \\
&= [\, I_{dr} - I_{dr-ref} \quad I_{qr} - I_{qr-ref} \,]^T, \qquad (37)
\end{aligned}
$$

Differentiating Eq. 37 with respect to time yields

$$
\dot{e} = \dot{x} - \dot{x}_{ref} = f(x) + hu + d - \dot{x}_{ref} \qquad (38)
$$

The proposed fractional order sliding surface vector is defined as $S_i = [\, S_1 \;\; S_2 \,]^T$

$$
\begin{bmatrix} S_1 \\ \dot{S}_1 \\ S_2 \\ \dot{S}_2 \end{bmatrix} = \begin{bmatrix} c_1 D^{-\alpha}e_1 + c_2 D^{\alpha}|e_1|^{\gamma}\mathrm{sgn}(e_1) \\ c_1 D^{1-\alpha}e_1 + c_2\gamma D^{\alpha}|e_1|^{\gamma-1}\dot{e}_1 \\ c_3 D^{-\alpha}e_2 + c_4 D^{\alpha}|e_2|^{\gamma}\mathrm{sgn}(e_2) \\ c_3 D^{1-\alpha}e_2 + c_4\gamma D^{\alpha}|e_2|^{\gamma-1}\dot{e}_2 \end{bmatrix} \qquad (39)
$$

In eq. 39, c_1, c_2, c_3 c_4 and γ are positive constants while α represents the order of the fractional operator i.e. $\alpha \in (0, 1)$. By applying the fractional operator $D^{-\alpha}$ to the 2nd and 4th row ($\dot{S}_1$, $\dot{S}_2$) of the Eq. (39) one obtains

$$
\begin{bmatrix} D^{1-\alpha}S_1 \\ D^{1-\alpha}S_2 \end{bmatrix} = \begin{bmatrix} c_1 D^{1-2\alpha}e_1 + c_2\gamma|e_1|^{\gamma-1}\dot{e}_1 \\ c_3 D^{1-2\alpha}e_2 + c_4\gamma|e_2|^{\gamma-1}\dot{e}_2 \end{bmatrix} \qquad (40)
$$

In Eq. 40, the operator $D^{1-\alpha}$ represents the fractional derivative term. For simplicity it is represented as $D^{\bar{\alpha}}$. By combining Eq. 38 and 40 one obtains

$$
D^{\bar{\alpha}}S_i = \begin{bmatrix} D^{\bar{\alpha}}S_1 \\ \\ D^{\bar{\alpha}}S_2 \end{bmatrix} = \begin{bmatrix} c_1 D^{1-2\alpha}e_1 + c_2\gamma|e_1|^{\gamma-1}(f_1(x) \\ \quad + h_1u_1 + d_1 - \dot{I}_{dr-ref}) \\ c_3 D^{1-2\alpha}e_2 + c_4\gamma|e_2|^{\gamma-1}(f_2(x) \\ \quad + h_2u_2 + d_2 - \dot{I}_{qr-ref}) \end{bmatrix} \qquad (41)
$$

In Eq. 41 the disturbance vector is represented as $d = [d_1 d_2]$. Using Eq. 41 the proposed control law is defined as $u = u_{eq} + u_s - \hat{d}$.

$$
\begin{aligned}
u_{eq} &= \begin{bmatrix} u_{eq1} \\ u_{eq2} \end{bmatrix} \\
&= \begin{bmatrix} h_1^{-1}(-f_1(x) + \dot{I}_{dr-ref} - \frac{c_1}{\gamma c_2}|e_1|^{1-\gamma}D^{1-2\alpha}e_1) \\ h_2^{-1}(-f_2(x) + \dot{I}_{qr-ref} - \frac{c_3}{\gamma c_4}|e_2|^{1-\gamma}D^{1-2\alpha}e_2) \end{bmatrix} \qquad (42)
\end{aligned}
$$

$$
u_s = \begin{bmatrix} u_{s1} \\ u_{s2} \end{bmatrix} = \begin{bmatrix} h_1^{-1}((-k_1(\mathrm{sgn}(S_1^p))) \\ h_2^{-1}((-k_2(\mathrm{sgn}(S_2^p))) \end{bmatrix} \qquad (43)
$$

In Eq. 42 and 43 u_{eq} represents the equivalent control which is used to compensate the nominal dynamics, while u_s is the robust term which is designed such that it will compensate the effects of the upper bounded lumped uncertainty in the plant model.

Stability Proof 1I: The new Lyapunov candidate function is expressed as $V_i = \frac{1}{2}S_i^2 + \frac{1}{2\zeta}(d-\hat{d})^2$. By applying the fractional operator $D^{\bar{\alpha}}$ to the function V_i yields

$$
D^{\bar{\alpha}}V_i = S_i D^{\bar{\alpha}}S_i + \frac{1}{\zeta}(d-\hat{d})D^{\bar{\alpha}}(d-\hat{d})
$$

$$+\left|\sum_{j=1}^{\infty}\frac{\Gamma(1+\bar{\alpha})}{\Gamma(1-j+\bar{\alpha})\Gamma(1+j)}D^{j}S_{i}D^{\bar{\alpha}-j}S_{i}\right|$$
$$+\left|\sum_{j=1}^{\infty}\frac{\Gamma(1+\bar{\alpha})}{\Gamma(1-j+\bar{\alpha})\Gamma(1+j)}D^{j}e_{d}D^{\bar{\alpha}-j}e_{d}\right| \quad (44)$$

From Eq. 44 the error term is expressed as $e_d = d - \hat{d}$ Eq. 44 can be further simplified using the inequality of Eq. 27 as following

$$D^{\bar{\alpha}}V_i \leq S_i D^{\bar{\alpha}}S_i + \frac{1}{\zeta}(d-\hat{d})D^{\bar{\alpha}}(-\hat{d}) + \lambda_3|S_i| + \lambda_4|e_d| \quad (45)$$

By combining u from Eq. 42, 43 in Eq-45 one obtains

$$D^{\bar{\alpha}}V_i \leq \begin{bmatrix} S_1 \\ S_2 \end{bmatrix}\begin{bmatrix} c_2\gamma|e_1|^{\gamma-1}(d_1-\hat{d}_1) \\ \quad -c_2\gamma|e_1|^{\gamma-1}h_1^{-1}((-k_1(\mathrm{sgn}(S_1^p))) \\ c_4\gamma|e_2|^{\gamma-1}((d_2-\hat{d}_2)) \\ \quad -c_2\gamma|e_1|^{\gamma-1}h_2^{-1}((-k_2(\mathrm{sgn}(S_2^p))) \end{bmatrix}$$
$$+\begin{bmatrix} \frac{1}{\zeta_1}(d_1-\hat{d}_1)D^{\bar{\alpha}}(-\hat{d}_1)+\lambda_{31}|S_1| \\ \quad +\lambda_{41}|e_{d1}| \\ \frac{1}{\zeta_2}(d_2-\hat{d}_2)D^{\bar{\alpha}}(-\hat{d}_2)+\lambda_{32}|S_2| \\ \quad +\lambda_{42}|e_{d2}| \end{bmatrix} \quad (46)$$

From Eq. 46, the following adaptive law is derived

$$\begin{bmatrix} D^{\bar{\alpha}}(\hat{d}_1) = \zeta_1 c_2\gamma|e_1|^{\gamma-1}S_1 \\ D^{\bar{\alpha}}(\hat{d}_2) = \zeta_2 c_4\gamma|e_1|^{\gamma-1}S_2 \end{bmatrix} \quad (47)$$

By combining Eq. 46 and 47 one obtains (48), as shown at the bottom of the next page

By letting $\begin{bmatrix} k_1 \geq \lambda_{31}+\lambda_{41} \\ k_2 \geq \lambda_{32}+\lambda_{42} \end{bmatrix}$ the term $D^{\bar{\alpha}}V_i \leq 0$

C. GRID SIDE CONTROLLER

The key objective of the grid side controller is to keep the voltage of the DC link constant irrespective of the magnitude and direction of the power flow through the rotor. In order to fulfill the objective, a vector control approach is employed using a reference frame oriented along the stator voltage or the grid voltage. In such a scheme the direct axis current is controlled in order to keep the DC link voltage constant [37].

In the stator voltage oriented reference frame, the d-axis is aligned with the grid voltage phasor V_s so $V_d = V_s$ and $V_q = 0$. Hence the active and reactive powers between the grid side converter and the grid is given as [2]

$$P = \frac{3}{2}(V_d I_d + V_q I_q) = \frac{3}{2}(V_d I_d) \quad (49)$$
$$Q = \frac{3}{2}(V_q I_d - V_d I_q) = -\frac{3}{2}(V_d I_q) \quad (50)$$

Where V_d, V_q represent the direct and quadrature components of the supply voltage, $I_d I_q$ are the direct and quadrature components of the grid side converter's currents. From Eq. 49 and 50 the active and reactive powers flow between the grid and grid side converter are proportional to the magnitude of I_d and I_q respectively. The change in DC power has to be equal to the active power flowing between the grid side controller and the grid. So the dynamics are expressed as

$$EI_{0s} = \frac{3}{2}V_d I_d \quad (51)$$
$$C\frac{dE}{dt} = I_{0s} - I_{0r} \quad (52)$$

In Eq. 51 and 52, E is the DC link voltage, I_{0r} is the current between the DC link and the rotor and I_{0s} is the current between the DC link and the grid. From equation (51) we have,

$$I_{0s} = \frac{3}{2E}V_d I_d \quad (53)$$

By replacing I_{0s} from Eq. (53) in (52) one obtains

$$\dot{E} = \frac{1}{C}\left(\frac{3}{2E}V_d I_d - I_{0r}\right)$$
$$\dot{E} = g(x)I_d - \frac{1}{C}I_{0r} \quad (54)$$

Where the function $g(x)$ can be defined as

$$g(x) = \frac{1}{C}\frac{3}{2E}V_d \quad (55)$$
$$g(x) = g_0(x) + \Delta g(x) \quad (56)$$

In Eq. 56 $g_0(x) = \frac{1}{C}\frac{3}{2E^*}V_d$, E^* represents the reference value of E and $\Delta g(x)$ is the uncertainty term. By replacing $g(x)$ from equation (56) into equation (54) yields

$$\dot{E} = (g_0(x) + \Delta g(x))I_d - \frac{1}{C}I_{0r} \quad (57)$$
$$\dot{E} = g_0(x)I_d - \frac{1}{C}I_{0r} + d_E \quad (58)$$

In Eq. 58, the term $d_E = \Delta g(x)I_d$ represents the uncertainty. By defining the voltage tracking error as

$$e_E = E - E^* \quad (59)$$

By differentiating Eq. (59) on both sides one obtains

$$\dot{e}_E = \dot{E} - \dot{E}^* \quad (60)$$

By replacing $\dot{E}$ from Eq. 58 in (60)

$$\dot{e}_E = g_0(x)I_d - \frac{1}{C}I_{0r} + d_E - \dot{E}^* \quad (61)$$

Define a fractional order sliding surface defined in (62)

$$S_E = c_7 D^{-\alpha}e_E + c_8 D^{\alpha}|e_E|^{\gamma}\mathrm{sgn}(e_E)$$
$$\dot{S}_E = c_7 D^{1-\alpha}e_E + c_8\gamma D^{\alpha}\underbrace{D^1|e_E|^{\gamma}\mathrm{sgn}(e_E)}$$
$$\dot{S}_E = c_7 D^{1-\alpha}e_E + c_8\gamma D^{\alpha}|e_E|^{\gamma-1}\dot{e}_E \quad (62)$$

Apply $D^{-\alpha}$ to both sides of $\dot{S}_E$ in (62) yields

$$D^{1-\alpha}S_E = c_7 D^{1-2\alpha}e_E + c_8\gamma|e_E|^{\gamma-1}\dot{e}_E \quad (63)$$

The operator $D^{1-\alpha}$ is represented as $D^{\bar{\alpha}}$. With this notation a more convenient form of the equation (63) is written as

$$D^{\bar{\alpha}}S_E = c_7 D^{1-2\alpha}e_E + c_8\gamma|e_E|^{\gamma-1}\dot{e}_E \quad (64)$$

By combining $\dot{e}_3$ from Eq. (61) in (64) one obtains

$$D^{\bar{\alpha}}S_E = c_7 D^{1-2\alpha}e_E + c_8\gamma\begin{pmatrix}|e_E|^{\gamma-1}g_0(x)I_d - \dfrac{|e_E|^{\gamma-1}}{C}I_{0r}\\ +|e_E|^{\gamma-1}d_E - |e_E|^{\gamma-1}\dot{E}^*\end{pmatrix} \tag{65}$$

Using Eq. 65 the control law for DC link voltage stabilization is derived

$$\begin{cases} I_d = I_{d-eq} + I_{d-s} - \hat{\phi} \\ I_{d-eq} = \dfrac{1}{g_0(x)}|e_s|^{1-\gamma}\{|e_s|^{\gamma-1}\dot{E}^* + \dfrac{|e_E|^{\gamma-1}}{C}I_{0r} \\ \qquad\qquad -|e_E|^{\gamma-1}d_E - \dfrac{c_7}{\gamma c_8}D^{1-2\alpha}(e_E)\} \\ I_{d-s} = \dfrac{1}{g_0(x)}|e_s|^{1-\gamma}(-\dfrac{k_{r4}}{\gamma c_8}(\mathrm{sgn}(S_E^p)) \end{cases} \tag{66}$$

In Eq. 66 c_7 *and* c_8 are the constant parameters, k_{r4} represents the discontinuous switching gain. From Eq. 65 the term $|e_E|^{\gamma-1}d_E = \phi$ and $\hat{\phi}$ represents the estimated value of the uncertainty term.

Stability Proof 3: The Lyapunov function is defined as, $V_E = \frac{1}{2}S_E^2 + \frac{1}{2\rho}(\phi - \hat{\phi})^2$. Apply the fractional operator $D^{\bar{\alpha}}$ to V_E yields

$$\begin{aligned} D^{\bar{\alpha}}V_E = {} & S_E D^{\bar{\alpha}}S_E + \frac{1}{\rho}(\phi-\hat{\phi})D^{\bar{\alpha}}(\phi-\hat{\phi}) \\ & + \left|\sum_{j=1}^{\infty}\frac{\Gamma(1+\bar{\alpha})}{\Gamma(1-j+\bar{\alpha})\Gamma(1+j)}D^j S_E D^{\bar{\alpha}-j}S_E\right| \\ & + \left|\sum_{j=1}^{\infty}\frac{\Gamma(1+\bar{\alpha})}{\Gamma(1-j+\bar{\alpha})\Gamma(1+j)}D^j e_\phi D^{\bar{\alpha}-j}e_\phi\right| \end{aligned} \tag{67}$$

In Eq. 67, $e_\phi = \phi - \hat{\phi}$. It is assumed that the unknown parameter ϕ in Eq. 66 is represented by its upper bound constant value. So Eq.67 can be simplified as

$$D^{\bar{\alpha}}V_E \le S_E D^{\bar{\alpha}}S_E\frac{1}{\rho}(\phi-\hat{\phi})D^{\bar{\alpha}}(-\hat{\phi}) + \lambda_5|S_E| + \lambda_6|e_\phi| \tag{68}$$

By following the same steps as given in the stability proof 1 and II, the adaptive control law is derived as

$$D^{\bar{\alpha}}\hat{\phi} = \rho c_8\gamma S_E \tag{69}$$

Combining Eq. 68 and 69 yields the following results: $D^{\bar{\alpha}}V_E \le -k_{r4}S_E(\mathrm{sgn}(S_E^p)) + \lambda_5|S_E| + \lambda_6|e_\phi|$ By letting $k_{r4} \ge \lambda_1 + \lambda_2$, Eq. 102 is $D^{\bar{\alpha}}V_E \le 0$

Remark 1: The derivation of the classical SMC is shown in Appendix B. For a comparative analysis about the robustness, convergence time and chattering in control signal, all control methods are applied under the same test conditions as discussed in the results and discussion section. The novel

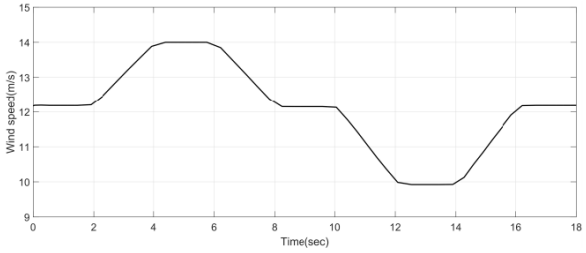

FIGURE 2. Wind profile.

points of the proposed method include the selection of novel fractional order surfaces, novel fractional order adaptive laws and the stability and convergence proof using fractional order Lyapunov theorem.

VI. RESULTS AND DISCUSSIONS

In this section, numerical simulations are presented to demonstrate the effectiveness of the proposed adaptive fractional order terminal sliding mode controller for a DFIG based wind energy conversion system. To choose the parameters of the proposed control system, MATLAB/Simulink response optimization tool box is used and the integral absolute error criteria are used to minimize the objective function. The details of the parameters selection using response optimization toolbox are given in [43]. Based on it the parameters for the proposed rotor side control system are chosen as $c_1 = 200, c_2 = 0.5, c_3 = 200, c_4 = 0.5, c_5 = 300$ *and* $c_6 = 0.9$. The switching gains are chosen as $k_{r1} = 0.1, k_{r2} = 0.1, k_{r3} = 0.1$, and the learning rates for the adaptive laws are selected as $\eta_1 = 100, \eta_2 = 100, \eta_3 = 100$. Similarly the design parameters for the grid side controller are chosen as $c_7 = 100, c_8 = 1, k_{r4} = 0.1, \rho = 1050$. The fractional order alpha is chosen as $\alpha = 0.8$. The nominal parameters of the DFIG and wind turbine system are listed in the Appendix A. Fig.2 show the wind profile used in simulation. The following two cases are discussed in details for both the rotor side as well as the grid side converter's control.

A. CASE 1

In case 1 it is considered that system is running under ideal condition without any parametric uncertainty and external disturbance.

Fig. 3(a) and 3(b) show the rotor speed tracking performance and speed tracking error. Under the ideal condition, proposed control scheme offers accurate speed tracking as compared to the SMC, and PI controller. **Fig**. 4(a) and 4(b) show the DFIG stator's active and reactive power comparison. It can be seen that the tracking performance of the proposed controller is good and after a short transient time, the reactive

$$D^{\bar{\alpha}}V_i \le \begin{bmatrix} -c_2\gamma|e_1|^{\gamma-1}S_1 h_1^{-1}((-k_1(\mathrm{sgn}(S_1^p))) + \lambda_{31}|S_1| + \lambda_{41}|e_{d1}| \\ -c_2\gamma|e_1|^{\gamma-1}S_2 h_2^{-1}((-k_2(\mathrm{sgn}(S_2^p))) + \lambda_{32}|S_2| + \lambda_{42}|e_{d2}| \end{bmatrix} \tag{48}$$

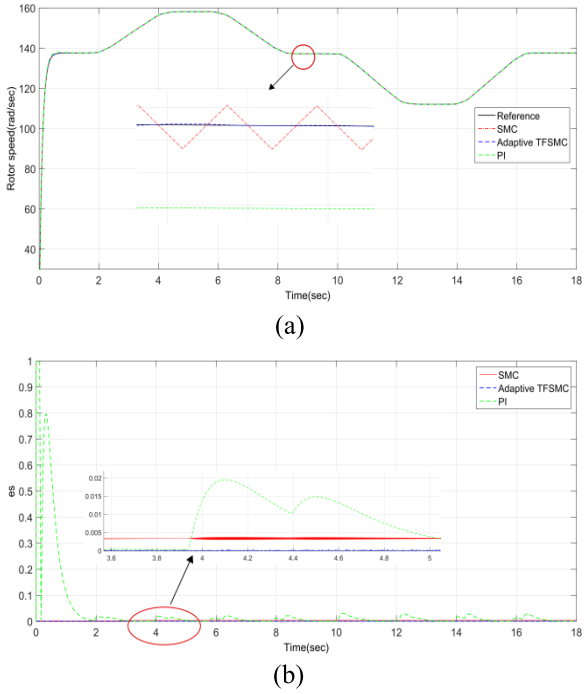

FIGURE 3. (a) Rotor speed (b) Speed tracking error.

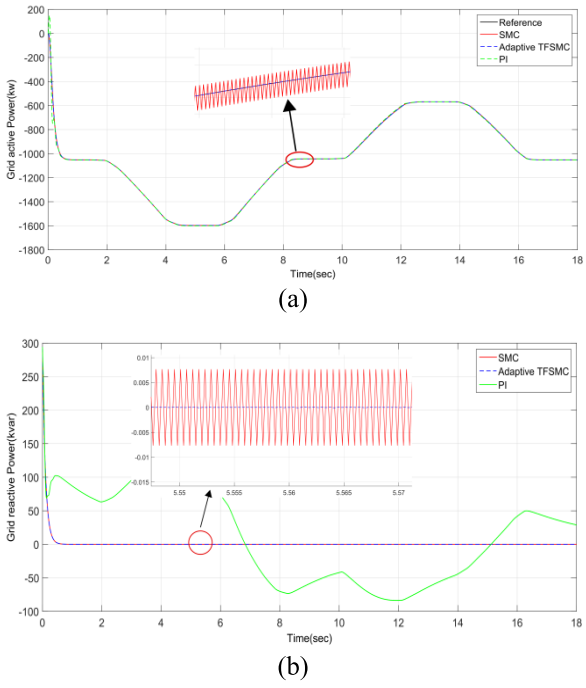

FIGURE 4. (a) Active power (b) Reactive power.

power approaches to zero. On the other hand, PI controller shows deviation from the reference reactive power due to the inherent nonlinearities in the DFIG model and reactive power cannot converge to zero.

As discussed earlier, that active power is controlled through q-component of the current and reactive power through

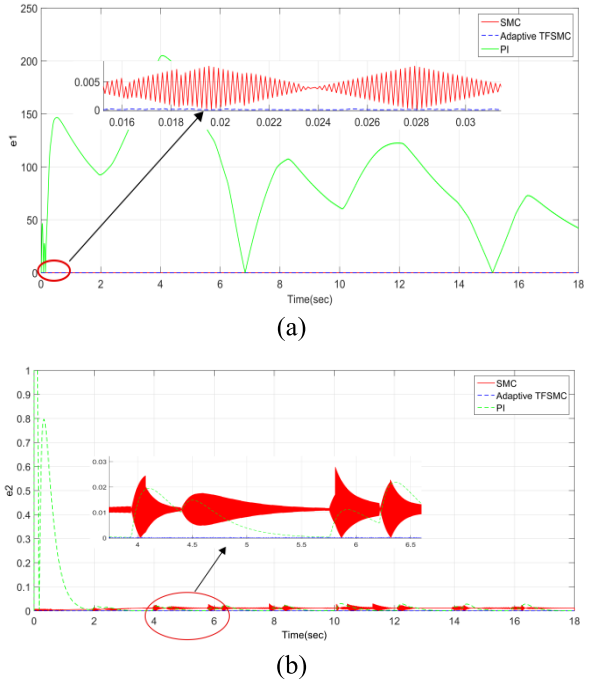

FIGURE 5. (a), (b) current controllers tracking error comparison.

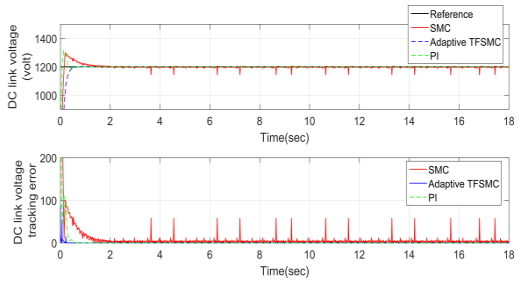

FIGURE 6. DC Link voltage and DC link voltage tracking error.

d-component. **Fig.**5 (a) and (b) show the current tracking error of the current controllers. From the figures it is obvious that the steady state error is less in the case of the adaptive fractional terminal SMC whereas classical SMC exhibit oscillations over the steady state.

Fig. 6 shows the DC link voltage tracking performance and voltage tracking errors. Under the ideal conditions, the proposed control scheme maintains constant DC link voltage as compared to the SMC and PI controllers.

Fig. 7 and **Fig**. 8 show the sliding surface convergence and control input comparisons for the rotor side controllers. Similarly **Fig**. 9 shows the same comparison for grid side controller. From **Fig**. 7 and **Fig**. 9 it is clear that adaptive fractional terminal SMC offers shortest convergence time whereas classical SMC exhibits oscillations.

Similarly from the control input comparison results depicted in **Fig**. 8 and **Fig**. 9 it can be concluded that adaptive fractional terminal SMC ensures fast dynamic response with minimum chattering as compared to SMC for both rotor side control as well as grid side control.

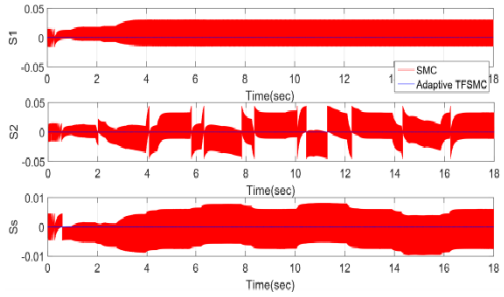

FIGURE 7. Sliding Surfaces convergence.

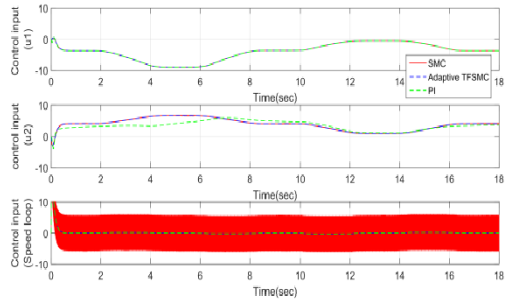

(a)

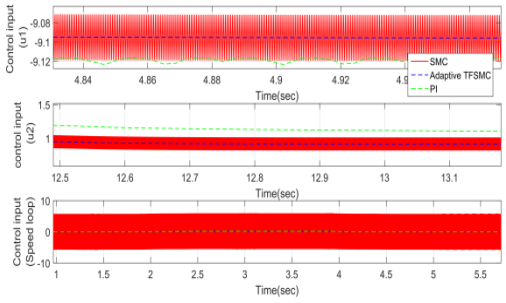

(b)

FIGURE 8. (a), (b) Control inputs comparisons.

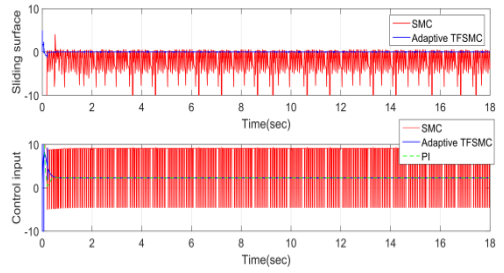

FIGURE 9. Sliding surface and control input comparison for grid side control.

B. CASE 2

To illustrate the effectiveness of the proposed adaptive fractional terminal SMC, the closed loop system's response is examined under parametric variation and external disturbances. From the previous analysis it is assumed that the lumped uncertainty d consists of parameter variations and external disturbances. In our case we have assumed that there is 25% variation in the system's nominal parameter values and a sinusoidal disturbance is assumed to be acting on the

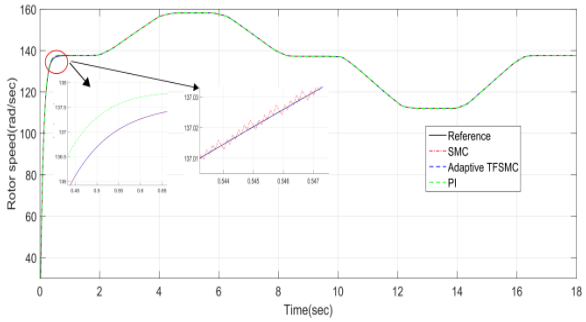

(a)

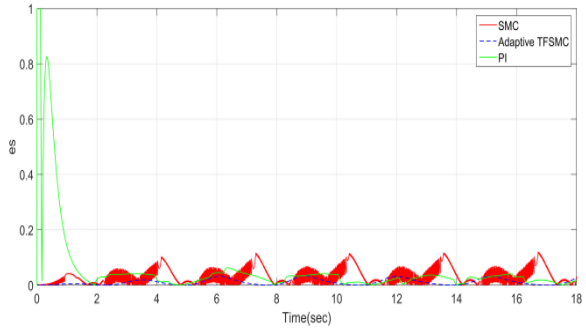

(b)

FIGURE 10. (a) Rotor speed, (b) Speed tracking error.

speed as well as current loops. Mathematically it is expressed as

$$\begin{cases} \dot{x} = F(x) + Hu = f(x) + hu + d \\ d = 25\% f(x) + 25\% hu + 20\sin(wt) \end{cases}$$

Similarly in section 4.3 it is assumed that the lumped uncertainty term d_E consists of the parameter variations and external disturbances. A 25% variation in the system's nominal parameters with a sinusoidal disturbance is considered to be acting on grid side controller.

$$\{d_E = 25\% g(x) + 5\sin\ (wt).$$

The sinusoidal disturbance term is added which simulates the effect of slow frequency power oscillations [40], [41].

Performance of the proposed controller is compared with SMC and PI controller. **Fig**.10 (a) and (b) shows the speed and speed error tracking performance of the proposed control system. From the numerical results it is clear that the proposed control scheme is more robust under the uncertainties in the system. Speed tracking errors of the proposed controller converge faster as compared to the other controllers.

Fig.11 (a) and (b) show the active and reactive power integrating capability of the DFIG system under different controllers. It can be seen that the tracking performance of the proposed controller under parametric uncertainties and external disturbance are much better and after a short transient time, reactive power approaches to zero, which is not true for SMC and PI controllers respectively. Current controllers tracking error comparison is shown in **Fig**. 12 (a) and (b). It can be concluded that tracking error of the proposed control

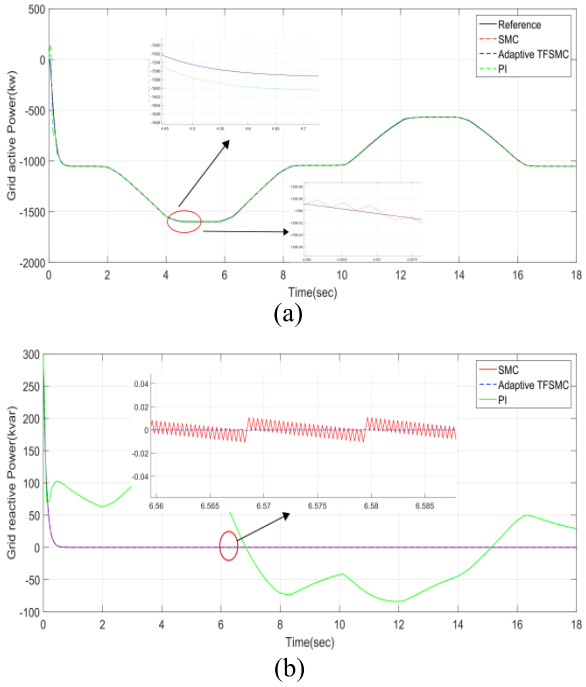

FIGURE 11. (a) Active power (b) Reactive power.

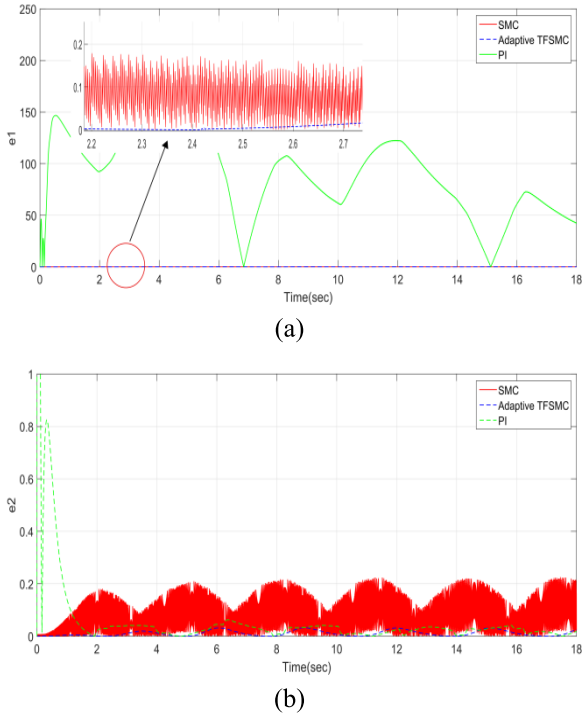

FIGURE 12. (a), (b) current controllers tracking error comparison.

scheme converges to zero more quickly as compared to the SMC and PI controllers.

Fig. 13 shows the DC link voltage tracking performance and tracking errors. It can be concluded that there is an increase in settling time of the SMC and the PI controllers whereas adaptive fractional terminal SMC shows robust performance and tracks the reference with minimum settling time.

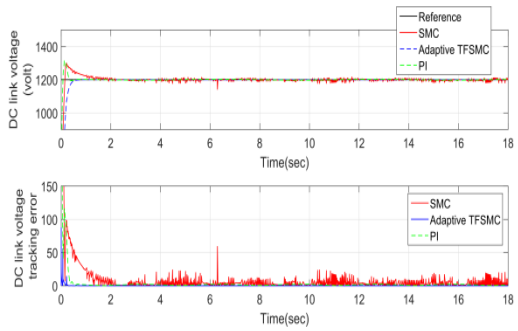

FIGURE 13. DC Link voltage and DC link voltage tracking error.

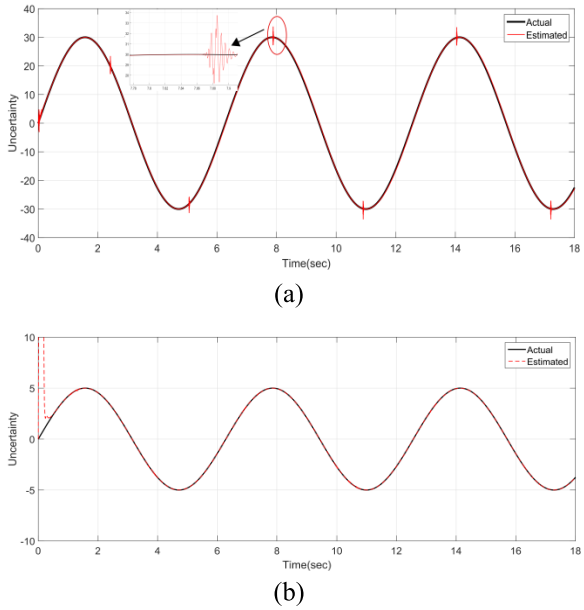

FIGURE 14. (a), (b) Uncertainty estimations.

Estimated lumped uncertainty using adaptive Terminal Fraction SMC (TFSMC)

This section presents the results and discussion related to the online estimation of the lumped uncertainty using fractional terminal order adaptive laws derived in the previous sections. Fig. 14(a) shows the estimated uncertainty of rotor side controllers when $\{d = 25\%f(x) + 25\%hu + 20\sin(wt)$. From the numerical results, the uncertainty approximation error is negligibly small. Similarly Fig. 14(b) shows the estimated uncertainty of grid side controller when $\{d_E = 25\%g(x) + 5\sin(wt)$. From the numerical results, it can be concluded that the uncertainty approximation error is very small.

VII. CONCLUSIONS

In this paper, two variants of the sliding mode controllers including classical SMC and adaptive fractional terminal SMC are derived for the rotor and grid side converters. Both variants are compared with classical PI controller under different test conditions such as the parametric uncertainty, external disturbances. From the numerical simulation results presented, it is concluded that the proposed adaptive

TABLE 1. System parameter.

DFIG		Wind Turbine	
Parameter	Value	Parameter	Value
Power	2Mw	Blade radius	35 m
Voltage	700V	Gear ratio	62.5
$L_s = L_r$	0.005305 H	λ_{opt}	6.325
M	0.0051839 H		
f_f	0.00015 $N\,m\,s^{-2}$		
$P(Pole\ pairs)$	3		
J	765.6 $kg\,/\,m^2$		
DC link voltage(E)	1200 Volt		
DC link Capacitor	0.01 farad		
Frequency	50 Hz		

fractional terminal sliding mode controllers (both rotor and grid side) exhibit the fastest transient response and convergence property at all test conditions. Another performance evaluation criterion is the level of the control signal chattering. From the numerical results it is concluded that the proposed adaptive fractional order terminal sliding mode controller exhibits the minimum chattering level in the control signal.

APPENDIX A

The DFIG based wind turbine system nominal parameter values are given in table 1

APPENDIX B (SMC)

A. SPEED CONTROLLER DERIVATION

Classical sliding surface for speed controller is given as

$$S_3 = c_5 e_3 + c_6 \int e_3 \tag{B1}$$

By using the dynamic model of the speed and adopting the same procedure as above, the control law can be chosen as

$$\begin{cases} T_{em} = T_{em-eq} + T_{em-s} \\ T_{em-eq} = J(\dot{\Omega}_{r-ref} - d_3 - (\dfrac{c_6}{c_5} e_3)) \\ T_{em-s} = J(-\dfrac{k_{r3}}{c_5}(\mathrm{sgn}(s_3))) \end{cases} \tag{B2}$$

Where c_5 *and* c_6 are designed parameters and k_{r3} is discontinuous switching gain which is to be chosen later.

B. CURRENT CONTROLLER DERIVATION

The classical sliding surface vector for current loop is given as $S_1 = [\,S_1\ S_2\,]^T$

$$S = \begin{bmatrix} S_1 \\ S_2 \end{bmatrix} = \begin{bmatrix} c_1 e_1 + c_2 \int e_1 \\ c_3 e_2 + c_4 \int e_2 \end{bmatrix} \tag{B3}$$

Where c_1, c_2, c_3 and c_4 are positive tuning parameters. By using the rotor side system model and adopting the same procedure as above, the current loop controllers are derived as

$$u_{eq} = \begin{bmatrix} u_{eq1} \\ u_{eq2} \end{bmatrix} = \begin{bmatrix} h^{-1}(-f(x) + \dot{I}_{dr-ref} - \dfrac{c_2}{c_1} e_1) \\ h^{-1}(-f(x) + \dot{I}_{qr-ref} - \dfrac{c_4}{c_3} e_1) \end{bmatrix} \tag{B4}$$

$$u_s = \begin{bmatrix} u_{s1} \\ u_{s2} \end{bmatrix} = \begin{bmatrix} h^{-1}(-\dfrac{k_{r1}}{c_1}\mathrm{sgn}(S_1)) \\ h^{-1}(-\dfrac{k_{r2}}{c_3}\mathrm{sgn}(S_2)) \end{bmatrix} \tag{B5}$$

C. SMC FOR GSC

Sliding surface is given as.

$$S_E = c_7 e_E + c_8 \int e_E \tag{B6}$$

By using the grid side nonlinear model and the procedure followed in the manuscript the control law can be chosen as

$$\begin{cases} I_d = I_{d-eq} + I_{d-s} \\ I_{d-eq} = \dfrac{1}{g_0(x)}\{\dot{E}^* + \dfrac{1}{C} I_{0r} - \dfrac{c_8}{c_7}(e_E)\} \\ I_{d-s} = \dfrac{1}{g_0(x)}(-\dfrac{k_{r4}}{c_7}(\mathrm{sgn}(S_E)) \end{cases} \tag{B7}$$

In Eq. B7, c_7 *and* c_8 are the constant parameters, k_{r4} represents the discontinuous switching gain.

REFERENCES

[1] R. McMahon, E. Abdi, A. Broekhof, P. Roberts, M. Tatlow, and S. Abdi, "Rotor parameter determination for the brushless doubly fed (induction) machine," *IET Electr. Power Appl.*, vol. 9, no. 8, pp. 549–555, 2015.

[2] H. Chaal and M. Jovanovic, "Direct power control of brushless doubly-fed reluctance machines," in *Proc. 5th IET Int. Conf. Power Electron., Mach. Drives (PEMD)*, Apr. 2010, pp. 1–6.

[3] *GLOBAL WIND REPORTS|GWEC*. Accessed: Mar. 19, 2017. [Online]. Available: http://www.gwec.net/publications/global-wind-report-2/

[4] B. C. Babu and K. B. Mohanty, "Doubly-fed induction generator for variable speed wind energy conversion systems-modeling & simulation," *Int. J. Comput. Elect. Eng.*, vol. 21, pp. 141–147, Feb. 2010.

[5] Y. Wang, L. Xu, and B. W. Williams, "Control of DFIG-based wind farms for network unbalance compensation," in *Proc. IEEE Power Electron. Spec. Conf.*, Jun. 2008, pp. 113–119.
[6] Y. Bekakra and D. B. Attous, "Optimal tuning of PI controller using PSO optimization for indirect power control for DFIG based wind turbine with MPPT," *Int. J. Syst. Assurance Eng. Manage.*, vol. 5, no. 3, pp. 219–229, 2013.
[7] R. Pena, R. Cardenas, J. Proboste, G. Asher, and J. Clare, "Sensorless control of doubly-fed induction generators using a rotor-current-based MRAS observer," *IEEE Trans. Ind. Electron.*, vol. 55, no. 1, pp. 330–339, Jan. 2008.
[8] I. Munteanu, N. A. Cutululis, A. Bratcu, and E. Ceangă, "Optimization of variable speed wind power systems based on a LQG approach," *Control Eng. Pract.*, vol. 13, no. 7, pp. 903–912, 2005.
[9] F. E. V. Taveiros, L. S. Barros, and F. B. Costa, "Back-to-back converter state-feedback control of DFIG (doubly-fed induction generator)-based wind turbines," *Energy*, vol. 89, pp. 896–906, Sep. 2015.
[10] H. Moradi and G. Vossoughi, "Robust control of the variable speed wind turbines in the presence of uncertainties: A comparison between H_∞ and PID controllers," *Energy*, vol. 90, pp. 1508–1521, Oct. 2015.
[11] O. Soares, H. Gonçalves, A. Martins, and A. Carvalho, "Neural networks based power flow control of the doubly fed induction generator," in *Proc. Int. Conf. Power Eng., Energy Elect. Drives*, Mar. 2009, pp. 599–604.
[12] B. Hamane, M. Benghanemm, A. Bouzid, A. Belabbes, M. Bouhamida, and A. Draou, "Control for variable speed wind turbine driving a doubly fed induction generator using fuzzy-PI control," *Energy Procedia*, vol. 18, pp. 476–485, Jan. 2012.
[13] B. Bossoufi *et al.*, "Robust adaptive backstepping control approach of DFIG generators for wind turbines variable-speed," in *Proc. Int. Renew. Sustain. Energy Conf. (IRSEC)*, Oct. 2014, pp. 791–797.
[14] R. K. Patnaik, P. K. Dash, and K. Mahapatra, "Adaptive terminal sliding mode power control of DFIG based wind energy conversion system for stability enhancement," *Int. Trans. Elect. Energy Syst.*, vol. 26, no. 4, pp. 750–782, 2015.
[15] E. Bounadja, A. Djahbar, and Z. Boudjema, "Variable structure control of a doubly fed induction generator for wind energy conversion systems," *Energy Procedia*, vol. 50, pp. 999–1007, Jan. 2014.
[16] G. Kaloi, J. Wang, and M. Baloch, "Active and reactive power control of the doubly fed induction generator based on wind energy conversion system," *Energy Rep.*, vol. 2, pp. 194–200, Nov. 2016.
[17] R. K. Patnaik and P. K. Dash, "Fast adaptive back-stepping terminal sliding mode power control for both the rotor-side as well as grid-side converter of the doubly fed induction generator-based wind farms," *IET Renew. Power Generat.*, vol. 10, no. 5, pp. 598–610, 2016.
[18] R. K. Patnaik and P. K. Dash, "Fast adaptive finite-time terminal sliding mode power control for the rotor side converter of the DFIG based wind energy conversion system," *Grids Netw.*, vol. 1, pp. 63–84, Mar. 2015.
[19] K. Boulâam and A. Boukhelifa, "Fuzzy sliding mode control of DFIG power for a wind conversion system," in *Proc. 16th Int. Power Electron. Motion Control Conf. Expo.*, Sep. 2014, pp. 353–358.
[20] S. E. B. Elghali, M. E. H. Benbouzid, T. Ahmed-Ali, J. F. Charpentier, and F. Mekri, "High-order sliding mode control of DFIG-based marine current turbine," in *Proc. 34th Annu. Conf. IEEE Ind. Electron.*, Nov. 2008, pp. 1228–1233.
[21] M. Benbouzid, B. Beltran, Y. Amirat, G. Yao, J. Han, and H. Mangel, "Second-order sliding mode control for DFIG-based wind turbines fault ride-through capability enhancement," *ISA Trans.*, vol. 53, no. 3, pp. 827–833, May 2014.
[22] M. Taleb, F. Plestan, and B. Bououlid, "Higher order sliding mode control based on adaptive first order sliding mode controller," *IFAC Proc. Volumes*, vol. 47, no. 3, pp. 1380–1385, 2014.
[23] P. K. Dash and R. Patnaik, "Adaptive second order sliding mode control of doubly fed induction generator in wind energy conversion system," *J. Renew. Sustain. Energy*, vol. 6, p. 053143, Oct. 2014.
[24] J. Bai and X. C. Feng, "Fractional-order anisotropic diffusion for image denoising," *IEEE Trans. Image Process.*, vol. 16, no. 10, pp. 2492–2502, Oct. 2007.
[25] K. S. Miller and B. Ross, *An Introduction to the Fractional Calculus and Fractional Differential Equations*, 1st ed. New York, NY, USA: Wiley, 1993.
[26] I. Podlubny, *Fractional Differential Equations*, 1st ed. San Diego, CA, USA: Academic, 1999.
[27] M. B. Delghavi, S. Shoja-Majidabad, and A. Yazdani, "Fractional-order sliding-mode control of islanded distributed energy resource systems," *IEEE Trans. Sustain. Energy*, vol. 7, no. 4, pp. 1482–1491, Oct. 2016.
[28] D. Matignon, "Stability properties for generalized fractional differential systems," *ESAIM, Proc.*, vol. 5, pp. 145–158, Dec. 1998.
[29] M. P. Aghababa, "A Lyapunov-based control scheme for robust stabilization of fractional chaotic systems," *Nonlinear Dyn.*, vol. 78, no. 3, pp. 2129–2140, 2014.
[30] C. Li and W. Deng, "Remarks on fractional derivatives," *Appl. Math. Comput.*, vol. 187, no. 2, pp. 777–784, 2007.
[31] F. Zhang and C. Li, "Stability analysis of fractional differential systems with order lying in (1,2)," *Adv. Difference Equ.*, vol. 2011, p. 213485, Dec. 2011.
[32] Z. Gao and X. Liao, "Improved Oustaloup approximation of fractional-order operators using adaptive chaotic particle swarm optimization," *J. Syst. Eng. Electron.*, vol. 23, no. 1, pp. 145–153, 2012.
[33] T. Burton, *Wind Energy Handbook*, 1st ed. Chichester, U.K.: Wiley, 2011.
[34] M. I. Martinez, G. Tapia, A. Susperregui, and H. Camblong, "Sliding-mode control for DFIG rotor- and grid-side converters under unbalanced and harmonically distorted grid voltage," *IEEE Trans. Energy Convers.*, vol. 27, no. 2, pp. 328–339, Jun. 2012.
[35] F. K. A. Lima, E. H. Watanabe, P. Rodriguez, and A. Luna, "A simplified model for wind turbine based on doubly fed induction generator," in *Proc. Int. Conf. Elect. Mach. Syst.*, Aug. 2011, pp. 1–6.
[36] S. M. Mozayan, M. Saad, H. Vahedi, H. Fortin-Blanchette, and M. Soltani, "Sliding mode control of PMSG wind turbine based on enhanced exponential reaching law," *IEEE Trans. Ind. Electron.*, vol. 63, no. 10, pp. 6148–6159, Oct. 2016.
[37] O. Barambones, J. Cortajarena, P. Alkorta, and J. M. de Durana, "A real-time sliding mode control for a wind energy system based on a doubly fed induction generator," *Energies*, vol. 7, no. 10, pp. 6412–6433, 2014.
[38] J. Yao, Z. Jiao, D. Ma, and L. Yan, "High-accuracy tracking control of hydraulic rotary actuators with modeling uncertainties," *IEEE/ASME Trans. Mechatronics*, vol. 19, no. 2, pp. 633–641, Apr. 2014.
[39] J. Yao, Z. Jiao, and D. Ma, "Extended-state-observer-based output feedback nonlinear robust control of hydraulic systems with backstepping," *IEEE Trans. Ind. Electron.*, vol. 61, no. 11, pp. 6285–6293, Nov. 2014.
[40] M. Asghar and Nasimullah. *Performance Comparison of Wind Turbine Based Doubly Fed Induction Generator System Using Fault Tolerant Fractional and Integer Order Controllers*. Accessed: May 19, 2017. [Online]. Available: http://dx.doi.org/10.1016/j.renene.2017.01.008
[41] J. Hu, Y. He, L. Xu, and B. W. Williams, "Improved control of DFIG systems during network unbalance using PI–R current regulators," *IEEE Trans. Ind. Electron.*, vol. 56, no. 2, pp. 439–451, Feb. 2009.
[42] T. Surinkaew, I. Ngamroo, and W. Nakawiro, "Robust power oscillation damper design for DFIG-based wind turbine," in *Proc. 10th Int. Conf. Elect. Eng./Electron., Comput., Telecommun. Inf. Technol.*, May 2013, pp. 1–6.
[43] N. Ullah, M. A. Ali, R. Ahmad, and A. Khattak, "Fractional order control of static series synchronous compensator with parametric uncertainty," *IET Generat., Transmiss. Distrib.*, vol. 11, no. 1, pp. 289–302, 2017.
[44] H. Li, K. L. Shi, and P. G. McLaren, "Neural-network-based sensorless maximum wind energy capture with compensated power coefficient," *IEEE Trans. Ind. Appl.*, vol. 41, no. 6, pp. 1548–1556, Nov./Dec. 2005.

NASIM ULLAH received the Ph.D. degree in mechatronics engineering from Beihang University, Beijing, China, in 2013. From 2006 to 2010, he was a Senior Design Engineer with IICS, Pakistan. He is currently an Associate Professor of electrical engineering with CECOS University of Emerging Science and Information Technology, Peshawar, Pakistan. His research interests include renewable energy, flight control systems, integer and fractional order modeling of dynamic systems, integer/fractional order adaptive robust control methods, fuzzy/NN, hydraulic and electrical servos, epidemic, and vaccination control strategies.

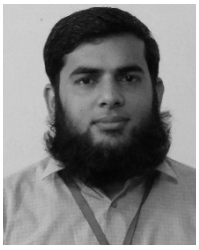

MUHAMMAD ASGHAR ALI was born in Dera Ismail Khan, Pakistan, in 1992. He received the B.Sc. degree in electrical engineering from University of Engineering and Technology and the M.Sc. degree in electrical power and control engineering from CECOS University Peshawar in 2013 and 2017, respectively. He is currently a Lecturer with Qurtuba University of Science and Information Technology, Dera Ismail Khan. His research interests include non-linear control systems, fractional order modeling and control of dynamic systems, power electronics, and renewable energy.

ASIER IBEAS was born in Bilbao, Spain, in 1977. He received the M.Sc. degree in applied physics and the Ph.D. degree in automatic control from University of the Basque Country, Spain, in 2000 and 2006, respectively. He is currently an Associate Professor of control systems with Autonomous University of Barcelona, Spain. He is also a Full Professor with Catalan Agency for Quality in Higher Education. He has authored over 130 contributions in international journals and conferences. He has supervised and is currently advising several doctoral theses and has participated in numerous research projects funded by regional and national agencies. His research interests include time-delayed systems, robust adaptive control, applications of artificial intelligence to control systems design, and nonconventional applications of control, such as to epidemic systems, supply chain management, and financial systems.

JORGE HERRERA received the degree in electronic engineering from University of Quindío, Colombia, in 2004, and the Ph.D. degree in industrial computing and advanced techniques of production from Universidad Autonoma de Barcelona, Spain, in 2011. He is currently a Full Professor with the Engineering Department, University Jorge Tadeo Lozano, Bogotá, Colombia. He is also the Director of the Industrial Engineering Program and the Director of the Master in Engineering Management. His active research lines are parametric identification and adaptive control.